

# EXECUTIVE FINAL PAPER

## L-band Observations of Soil and Trees in Freezing/Thawing Conditions – LOSTinFTC

Anna Kontu

Finnish Meteorological Institute

**Prepared by**  
**Approved by**  
**Reference**  
**Date of Issue**

**Anna Kontu**  
**Juha Lemmetyinen**  
**FR\_LOSTinFTC**  
**2022-11-09**

## 1 ABSTRACT

ESA Living Planet Fellowship project LOSTinFTC (L-band Observations of Soil and Trees in Freezing/Thawing conditions) studied the freezing of boreal forests at L-band and the thawing of soil with multifrequency passive microwave methods. The study applied data measured at the Arctic Space Centre of Finnish Meteorological Institute in Sodankylä, Finland, during 2020-2022 using two ESA ELBARA-II L-band radiometers (forest freezing) and in spring 2017 using ESA ELBARA-II L-band radiometer and FMI 10-36.5 GHz radiometer (soil thawing). During the project, a model describing the changes in the vegetation optical depth/transmissivity of a boreal forest canopy as a function of temperature was developed. The model was tested for temperatures between  $-30^{\circ}\text{C}$  and  $+10^{\circ}\text{C}$  with varying biomass and for tower-based and satellite measurements. Different stages of soil thaw and snowmelt in spring were identified from auxiliary data and detected from multifrequency microwave signals. A multifrequency method would allow for the detection of evolution of soil thaw and snowmelt above what current L-band methods are able to detect.

## 2 INTRODUCTION

Retrieval of soil parameters from satellite observations at L-band (1.4 GHz) in forested areas requires estimation of forest contribution to the measured signal. Typically, this is done using a simple  $\tau - \omega$  model, where forest properties are parameterised with vegetation optical depth (VOD)  $\tau$  and effective scattering albedo  $\omega$ . The SMOS soil moisture algorithm uses an approach where VOD estimate from L-band (L-VOD) at nadir is calculated from the yearly maximum leaf area index and time dependent components for canopy and understory contribution (Array Systems Computing Inc., 2011). The time dependent components vary seasonally to reflect changes in biomass during the growing season, but not daily and not with temperature changes. Recent measurement results (Li et al., 2019; Roy et al., 2020) show that the electrical properties of boreal forest canopy vary as a function of temperature due to gradual freezing of water. While the water in soil is frozen when soil temperature drops below  $0^{\circ}\text{C}$ , the water in trees can stay in liquid form down to  $-40^{\circ}\text{C}$  (Lintunen et al., 2013). The fractional amounts of liquid water and ice in trees affect the transmissivity of forest and hence the transmissivity of forest is dependent on air temperature. This changes the transmissivity of the forest canopy significantly between summer and winter conditions and especially during springtime when large ( $>20^{\circ}\text{C}$ ) variations between day- and nighttime temperature are common in the boreal region.

Passive microwave observations at L-band are able to detect soil freeze/thaw (F/T) status based on the differences in the electrical properties of ice and liquid water. Methods based on comparing the normalized polarization ratio (NPR)

$$NPR = \frac{T_B^V - T_B^H}{T_B^V + T_B^H} \quad (1)$$

of brightness temperature measurements at L-band H and V polarizations to summer and winter reference values have been developed for ESA SMOS (Rautiainen et al., 2016) and NASA SMAP (Derksen et al., 2017; Kim et al., 2019) missions. The NPR method is suitable for detecting autumn freezing, but during spring thawing the liquid water in melting snow confounds the signal from soil. F/T detection methods have also been developed for higher frequencies, mainly using 36.5 GHz V-polarization: The modified seasonal threshold algorithm (MSTA) (Kim et al., 2017) for SMMR, SMM/I and SSMIS data and the discriminant function algorithm (DFA) for AMSR-E and AMSR2 data (Wang et al., 2019). These methods are based on the relationship of 36.5 GHz TB to the temperature of the surface, but they react to changes in snowpack structure even more than the L-band methods due to sensitivity of the 36.5 GHz frequency to changes in snow structure. Multifrequency algorithms have been proposed for soil F/T detection (Muzalevskiy et al., 2022; Zhao et al., 2017), but with very preliminary results. (Muzalevskiy et al., 2022) proposes spectral gradients of brightness temperature and reflectivity for determining soil F/T state. This algorithm detects the timing of the F/T change more accurately than the NPR methods, but does not consider wet snow. The algorithm also performed poorly in Sodankylä and Saariselkä, the two measurement sites from Finland included in the study, due to the warm temperature (from  $0^{\circ}\text{C}$  to  $-4^{\circ}\text{C}$ ) and uneven freezing of soil. Reflectivity at polarization  $p$  and frequency  $f$  is calculated with

$$\Gamma_p(f) = 1 - \frac{T_B^p(f)}{T_B^V(6.9)} \quad (2)$$

where  $T_B^V(6.9)$  is used as an estimate for soil surface physical temperature.

This paper summarizes the work done in the Living Planet Fellowship project LOSTinFTC – L-band Observations of Soil and Trees in Freezing/Thawing Conditions. The two main objectives of the project were

- 1) Development of a model for boreal forest transmissivity at L-band as a function of temperature in freezing conditions
- 2) Study of methods for detecting soil freeze/thaw status at L-band in a boreal forest in spring thawing season

Data sets measured at the Arctic Space Centre of Finnish Meteorological Institute (FMI-ARC) in Sodankylä, Finland, was used in the study. Boreal forest L-VOD was measured with a tower-based setup using two ESA ELBARA-II radiometers. L-VOD calculated from measured brightness temperatures (TB) along with auxiliary reference measurements were used to develop the L-VOD model and validate it for different temperatures and forest biomasses. A different tower setup with L-Ka band radiometer measurements was used to study multifrequency TB of snow-covered soil in different stages of spring thaw and snowmelt.

## 3 METHODS

### 3.1 L-VOD measurements

Three different methods for calculating the L-VOD ( $\tau^p$ ) from the TB measurements were tested: the Mätzler method (Mätzler, 1994; Schwank et al., 2021), retrieval from two-stream (2S) model (Schwank et al., 2018), and retrieval using the  $\tau - \omega$  model (Roy et al., 2020). Mätzler method is a direct calculation from the downwelling below-canopy TB ( $T_{B2}^p$ ):

$$\tau^p = \cos(\theta) \cdot \ln\left(\frac{T_{veg} - T_{Bsky}}{T_{veg} - T_{B2}^p}\right), \quad (3)$$

where  $\theta = 50^\circ$  is the zenith angle of measurements,  $T_{veg}$  is canopy temperature (measured tree skin temperature) and  $T_{Bsky}$  is sky brightness temperature from ELBARA-II-A measurements. This approach does not consider emission from soil or scattering and reflections in the canopy, but is simple and fast. The other two methods include retrieval of L-VOD by minimizing error of observed and modelled TB. In contrast with the two others, the  $\tau - \omega$  method uses both above- and below-canopy measurements to retrieve  $\tau$  and  $\omega$  simultaneously. Since minimal differences between the methods were found, the Mätzler method (Eq. (3)) was used.

### 3.2 The L-VOD model

The developed L-VOD model describing the changes of forest vegetation optical depth as a function of canopy temperature is described in detail in (Schwank et al., 2021), but the most important equations are repeated here:

Nadir vegetation optical depth  $\tau$  at certain wavelength  $\lambda$  can be calculated, if canopy height  $h_c$  and permittivity  $\epsilon_c$  are known:

$$\tau_c = h_c \cdot \frac{4\pi}{\lambda} \cdot \text{Im}\sqrt{\epsilon_c}. \quad (4)$$

Forest canopy is a mixture of wood and air. At L-band, needles are transparent, and the main contribution comes from branches and other small canopy constituents (SCC). Canopy permittivity  $\epsilon_c$  is

$$\epsilon_c = \epsilon_{air} + \frac{(\epsilon_{wood} - \epsilon_{air}) \cdot (\epsilon_{wood} + 5 \cdot \epsilon_{air}) \cdot v_{SCC}}{3 \cdot (\epsilon_{wood} + \epsilon_{air}) - 2 \cdot (\epsilon_{wood} - \epsilon_{air}) \cdot v_{SCC}}, \quad (5)$$

where  $\epsilon_{air} = 1$  and  $\epsilon_{wood}$  are the relative permittivities of air and wood material, respectively, and  $v_{SCC}$  is the fraction of small canopy constituents of the total biomass. Trees can be modelled electromagnetically as a combination of water (the H<sub>2</sub>O phase, either liquid or frozen), air and wood

cells. Therefore, the relative permittivity of wood material ( $\epsilon_{wood}$ ) can be calculated from the permittivities of the H<sub>2</sub>O phase ( $\epsilon_{H_2O}$ ), wood cells ( $\epsilon_{woodcell}$ ) and air, and their respective fractional amounts, described with  $v_{H_2O}$  and porosity ( $por$ ):

$$\epsilon_{wood} = v_{H_2O} \cdot \epsilon_{H_2O} + (1 - por) \cdot \epsilon_{woodcell} + (por - v_{H_2O}) \cdot \epsilon_{air}. \quad (6)$$

The H<sub>2</sub>O phase consists of liquid water and frozen ice. Permittivity of water can be calculated using equations from (Klein & Swift, 1977). Real part of ice permittivity can be calculated with (Mätzler, 1987), and the imaginary part with (Mätzler, 2006). Their fractional amounts depend on canopy temperature. In (Schwank et al., 2021), an exponential function was used to calculate the fraction of liquid water of the H<sub>2</sub>O phase:

$$v_{water} = \begin{cases} 1 & , T_c > 0 \\ \exp(T_c/T_m), T_c \leq 0 \end{cases} \quad (7)$$

where  $T_m$  is an empirical fitting parameter (rate of freezing).

In its original form, the L-VOD model includes four optimization parameters: imaginary part of permittivity of wood cells ( $\epsilon_{woodcell}$ ), salinity of cell water ( $S_{water}$ ), water content of wood material ( $WC_{wood}$ ) and melting temperature ( $T_m$ ). Two of these, namely  $S_{water}$  and  $WC_{wood}$ , affect mainly when  $T_c > 0^\circ\text{C}$ . They both scale L-VOD and change the curvature of L-VOD to opposite directions.  $T_m$  affects the curvature of L-VOD when  $T_c < 0^\circ\text{C}$ . Wood-cell permittivity  $\epsilon_{woodcell}$  scales L-VOD in all temperatures. However,  $\epsilon_{woodcell}$  can be fixed based on measurements. This leaves two fitting parameters ( $S_{water}$  and  $WC_{wood}$ ) for  $T_c > 0^\circ\text{C}$  and one ( $T_m$ ) that can be fitted in  $T_c < 0^\circ\text{C}$  after the other two have been fixed.

### 3.3 Soil thaw and snowmelt

Typically snow begins to melt from the surface when solar radiation heats the surface while most of the snowpack is still frozen. When air temperature increases, the whole snowpack starts melting and becomes wet. Water begins to infiltrate through snowpack to soil surface and the soil begins to thaw, but soil temperature stays at  $0^\circ\text{C}$  until the all the snow has melted. Only when snowpack disappears, soil temperature increases above  $0^\circ\text{C}$ . Frozen soil is defined as soil with temperature  $< 0^\circ\text{C}$ , while soil is thawed when its temperature is  $> 0^\circ\text{C}$ . Between these two states water from melting snowpack infiltrates through snowpack to soil surface and soil thawing begin. While these two states are fairly easy to detect using remote sensing methods, the liquid water in snow and soil surface are difficult to differentiate from the signal of thawed soil.

Reference data was used to identify different stages of snowmelt and soil thaw:

- 1) soil frost: soil is frozen, snow is dry
- 2) wet surface snow: soil is frozen, snow is mostly frozen but snow surface is moist during day
- 3) wet snow: soil is frozen, the whole snowpack is moist
- 4) soil thawing: liquid water on soil surface layers but temperature  $\leq 0^\circ\text{C}$ , moist snowpack
- 5) soil thawed: soil temperature above  $0^\circ\text{C}$ , snow disappeared

The data from ELBARA-II measurements (1.4 GHz) and SodRad-1 radiometer (10.65 GHz, 18.7 GHz, 36.5 GHz) were studied during the different stages of snowmelt and soil thaw. Individual channels, different channel combinations, NPR and spectral gradient of reflectivity were studied to find differences between the snow melt stages as a basis for a new multifrequency algorithm for detection of soil F/T status during snowmelt.

## 4 DATA

### 4.1 Forest canopy data set

The setup at the ICOS tower (presented in Figure 1), including two ESA ELBARA-II L-band radiometers (Schwank et al., 2010), was used to study the L-band signals of a sparse boreal coniferous forest. Measurements from two winter seasons (1 Oct 2020-1 May 2021, 14 Oct 2021-1 May 2022) were used.

# Living Planet Fellowship

Hourly elevation scans with both ELBARA-II's were performed. An automated system prevented measurements during any precipitation, and automated data processing scripts were used to remove RFI and other suspicious signals. The nominal azimuth direction of the ELBARA-II radiometers was changed in 2021 from one with low biomass to one with more biomass. Based on the forest inventory, the new direction represents the general biomass of the forest area at  $50^\circ$  incidence angle. Figure 2 shows the measured above- and below-canopy brightness temperatures for the two winters. The measurement of the above-canopy radiometer is very similar during the two winters, but the TB for the below-canopy radiometer is higher for the second winter due to more canopy biomass in the field of view.

Reference measurements included tree skin temperature and trunk permittivity sensors (GS3 from Decagon Inc., now part of Meter Group, USA) installed in five trees at 2 m height, soil temperature and permittivity profile from the nearby IOA site (Stevens HydraProbe II), air and soil temperature, snow water equivalent (Sommer Messtechnik SSG 1000) and snow depth (Campbell Scientific SR50). In addition, a forest inventory (coordinates, height, canopy height and breast height diameter of each tree (diameter > 5 cm) in the measurement area) was measured in the summer of 2019. All temperature and permittivity measurements are shown in Figure 3.

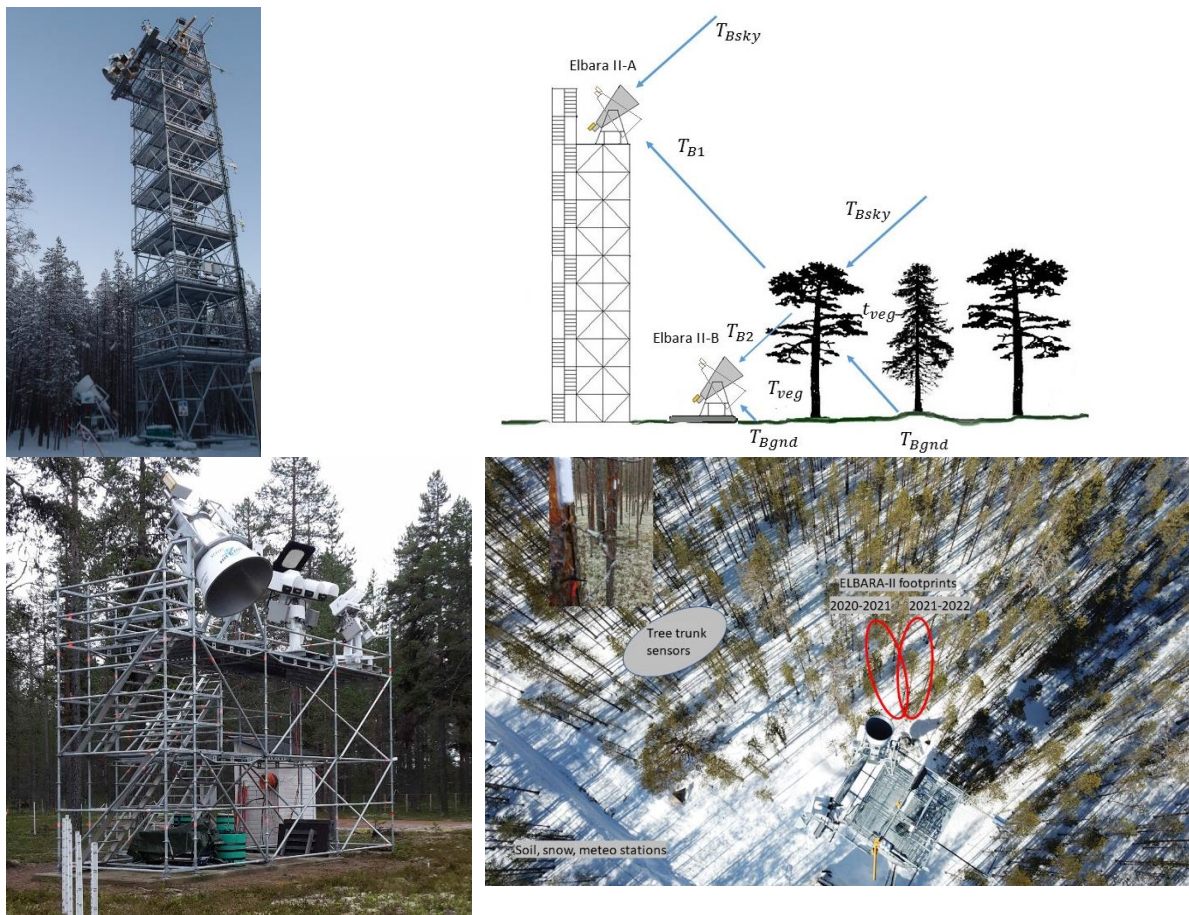


Figure 1: Forest canopy measurement setup (top left); Canopy measurement setup and measured variables (top right); Soil thawing measurement setup (bottom left); Aerial photo of the canopy measurement area with sensor locations and measurement directions (bottom right).

## 4.2 Soil thawing data set

Soil thawing was studied using a data set measured with two radiometers at the IOA site in 1 Feb-1 Jul 2017. The two towers are located in the same boreal forest about 600 m apart. The setup, shown in Figure 1, included one ESA ELBARA-II radiometer on a 5-m tower, along with two FMI SodRad radiometers for higher frequencies (10.65, 18.7, 21, 36.5, 89 and 150 GHz) measuring a forest opening with very similar soil and vegetation (lichen, lingonberry, heather) as the forest floor at the ICOS

tower site. This site was also equipped with reference measurements for soil moisture and temperature profile and snow temperature profile.

Same soil permittivity measurements (Stevens HydraProbe II) were used as with the ICOS tower data set. Snow temperature profile, snow depth and air temperature were measured also at the IOA tower site.

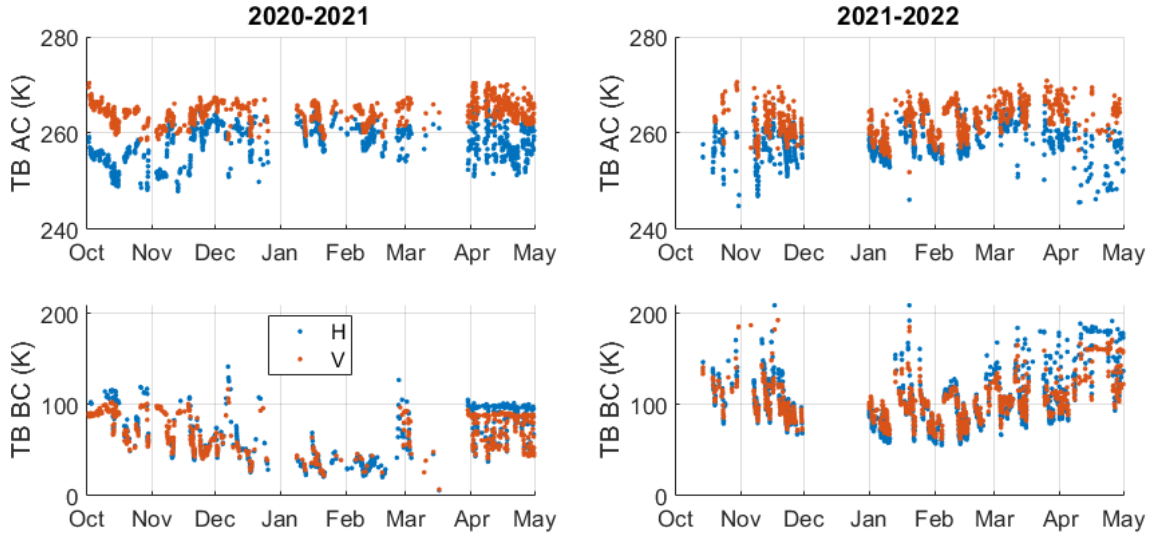


Figure 2: Measured brightness temperatures. Measurements were done also during summer, but only the wintertime data used in this project is shown. Higher values for TB BC in 2021-2022 are due to new measurement direction with more vegetation biomass.

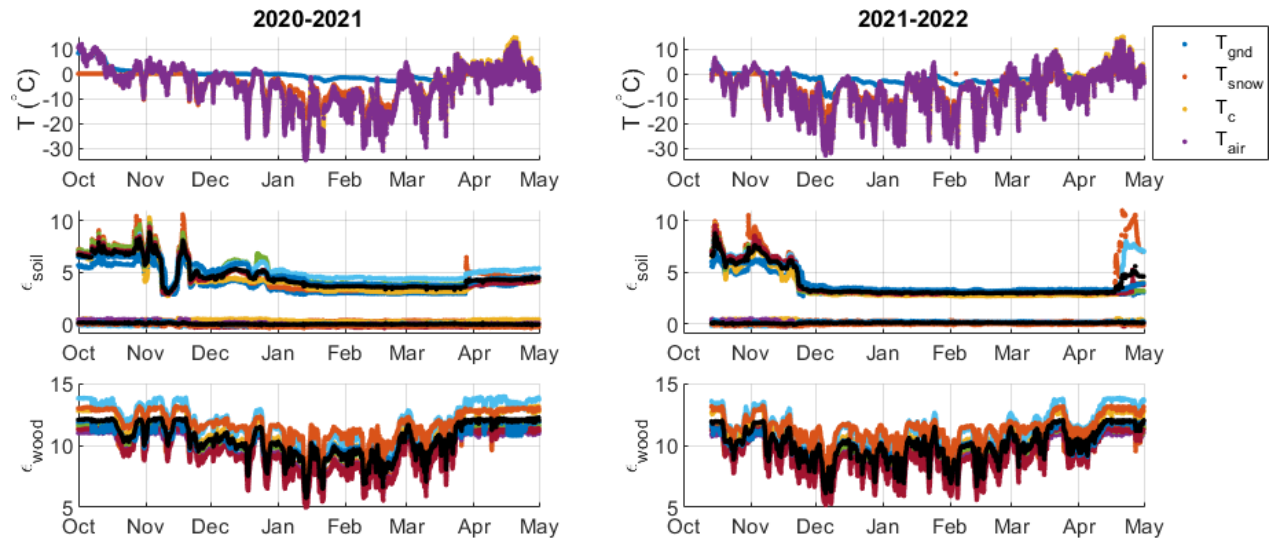


Figure 3: Temperatures and permittivities used with the ICOS tower data set. For permittivities, the colored lines show individual sensor measurements and the black lines are the mean values used in the study.

## 5 RESULTS

### 5.1 L-VOD model

Model parameter values used in this work are presented in Table 1. Realistic values that optimized the model but still resulted in reasonable wood permittivity were chosen. With the high number of model parameters, it could be fitted to measurements with other model and optimization parameters, but they would result in unrealistic wood permittivities. The two values of column-mass of dry canopy are based on calculations from the tree inventory data set. Two separate values for fraction of small canopy constituents are based on the fact that tree branches have a preferred horizontal position.

Table 1: L-VOD model parameter values

Parameter	Symbol	Value
Canopy height (m)	$h_c$	10
Column-mass of dry canopy (kg/m <sup>2</sup> )	$CM_{c,dry}$	5 (2019-2020) 15 (2020-2021)
Dry wood density (kg/m <sup>3</sup> )	$\rho_{wood,dry}$	300
Gravimetric fraction of small canopy constituents of the dry canopy	$m_{SCC}$	0.88 (H-pol) 0.8 (V-pol)
Wood porosity	$por$	0.6
Permittivity of wood cells	$\epsilon_{wc}$	$7 + 0.5j$

## Freezing of trees

One important part of the L-VOD model is the equation for the fraction of solid ice and liquid water in tree canopy as a function of temperature. This equation determines the permittivity of the canopy. This is very difficult to measure, so a simple exponential function was used in (Schwank et al., 2021) (Eq. (7)). The original formulation was based on measurements near 0°C. When the model was optimized for a wider temperature range, an equation of the form

$$v_{water} = \begin{cases} 1 & , T_c > 0 \\ 0.5 \cdot \left(1 - \frac{T_c + T_m}{T_c - T_m}\right) & , T_c \leq 0 \end{cases} \quad (8)$$

fit measured L-VOD behavior better.

The L-VOD model fitted using the two freezing equations to the measurements of 2020-2021 is shown in Figure 4 and the fitting parameter values are presented in Table 2 separately for the two winters. Model was fitted to both polarizations at the same time.

Table 2: Fitting parameters for the L-VOD model.

Parameter	Symbol	Value (orig)		Value (new)	
		2020-2021	2021-2022	2020-2021	2021-2022
Melting temperature (°C)	$T_m$	5.9	6.9	2.2	2.9
Salinity of wood cell water	$S$	4.9	0.0	4.9	0.0
Water content of wood	$W$	0.30	0.39	0.30	0.39

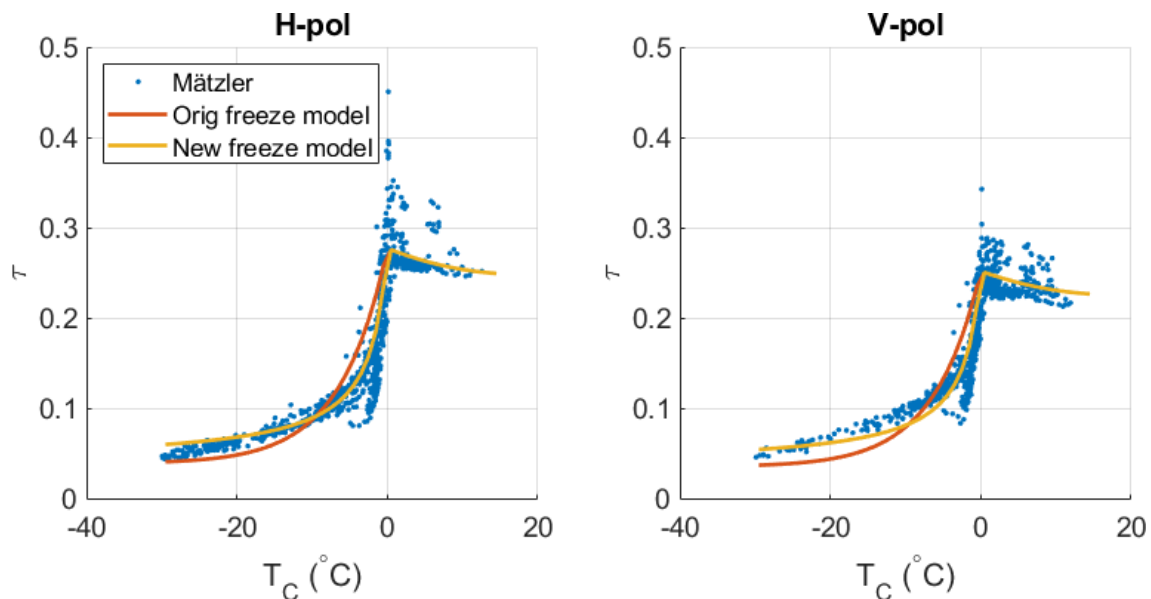


Figure 4: The L-VOD model fitted to measurements using two equations for tree freezing.

## L-VOD model and varying biomass

Figure 5 presents the results of fitting the L-VOD model to measurements from the winter of 2020-2021 using the low biomass value. For the winter of 2021-2022, the same model and optimization parameters were used, with the exception of higher biomass value. The model agrees very well with the second winter of measurements. Most significant differences can be seen when  $T_c > 0^\circ\text{C}$ , where the model gives higher L-VOD values than measurements. Partly this is explained with the fact that for the autumn of 2021, measurements in  $T_c > 0^\circ\text{C}$  are mostly missing, and the few measured values are from spring, when L-VOD is typically lower than in the autumn. The physical parameters (such as water content of wood) may change from year to year, so separate fitting for each year might still be necessary.

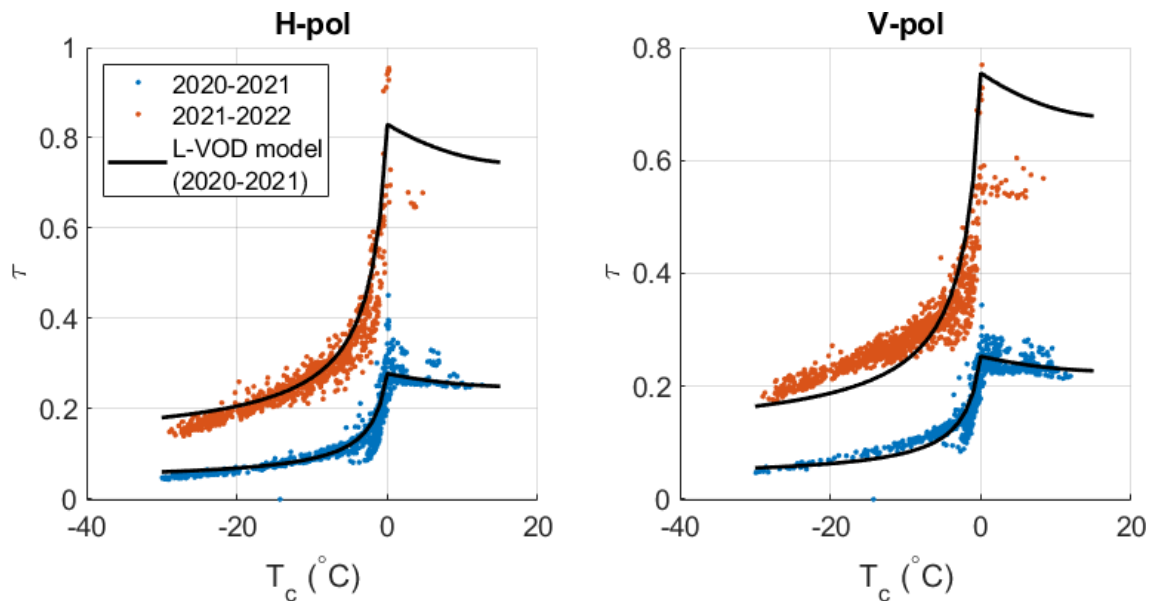


Figure 5: L-VOD measurements (Mätzler method) for two winters in different azimuth directions with the L-VOD model values.

## Simulated L-VOD timeseries

Figure 6 shows the timeseries of modelled and measured L-VOD for the two winters. The model is useful for gap-filling, since there are gaps in ELBARA-II measurements e.g. during radar measurements and precipitation events. It can also be used to simulate L-VOD, if no measurements are available. Measured L-VOD is higher in autumn (Oct-Dec) than in spring (Apr-May), showing that L-VOD is not only temperature dependent when  $T_c > 0^\circ\text{C}$ . This is also the reason why June-September time periods were left out of the analysis. However, during the winter, the model predicts L-VOD well.

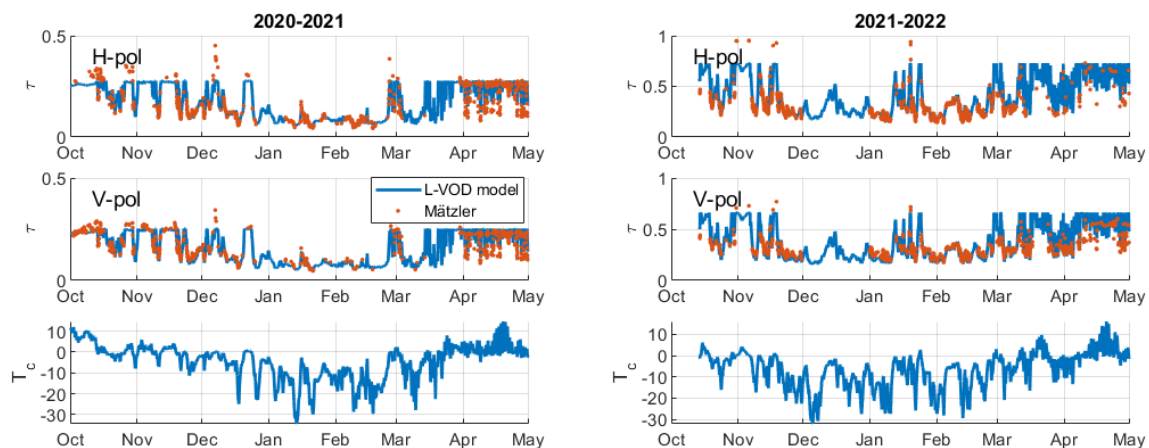


Figure 6: Simulated timeseries of L-VOD (blue) with measured values from the Mätzler model (red).

## 5.2 Snowmelt and soil thaw

Measurement data from spring 2017 are plotted in Figure 8. The five stages (1: frozen soil, dry snow, 2: wet surface snow during day, 3: frozen soil, wet snowpack, 4: moist (thawing) soil, wet snowpack, 5: warm (thawed) soil, no snow) of snowmelt and soil thawing are marked in the figure with vertical lines and identified in top panel. The four soil moisture sensors on the measurement footprint area react to temperature and moisture level changes at the same time, although the absolute measured values vary.

Figure 7 shows the measured brightness temperature data from the five stages for all frequencies and polarizations. Data from six consecutive days is plotted, except for stage 3, which is so short that only two days of data are shown. Stages 1 (frozen ground) and 5 (thawed ground) show a very small spread in measurements, making these easy to detect with either NPR (SMOS soil frost algorithm) or MSTA/DFA algorithms applying 36.5 V-pol. To get some further information about the soil thaw process, stages 2/3 (frozen soil, wet snow) and 4 (thawing soil) should be detected. In stage 1, the higher the frequency, the lower the measured TB, while in stage 5 the higher frequencies have higher TB. This change happens in different stages depending on frequency, so thawing soil could be detected e.g. from differences between 1.4 GHz and 10.65 or 18.7 GHz. This measurement result agrees with the findings of (Muzalevskiy et al., 2022). They also note that the timing of the sign change of spectral gradient coincides with soil thaw.

Another possible approach is shown in Figure 9, which shows normalized frequency ratios (similar to NPR, but for two frequencies, same polarization). Pairs 1.4-18.7 GHz and 1.4-36.5 GHz drop to negative values in stage 3 when snow is completely wet. This behaviour can also be modelled with MEMLS microwave snow model using the measurements shown in Figure 8 as input.

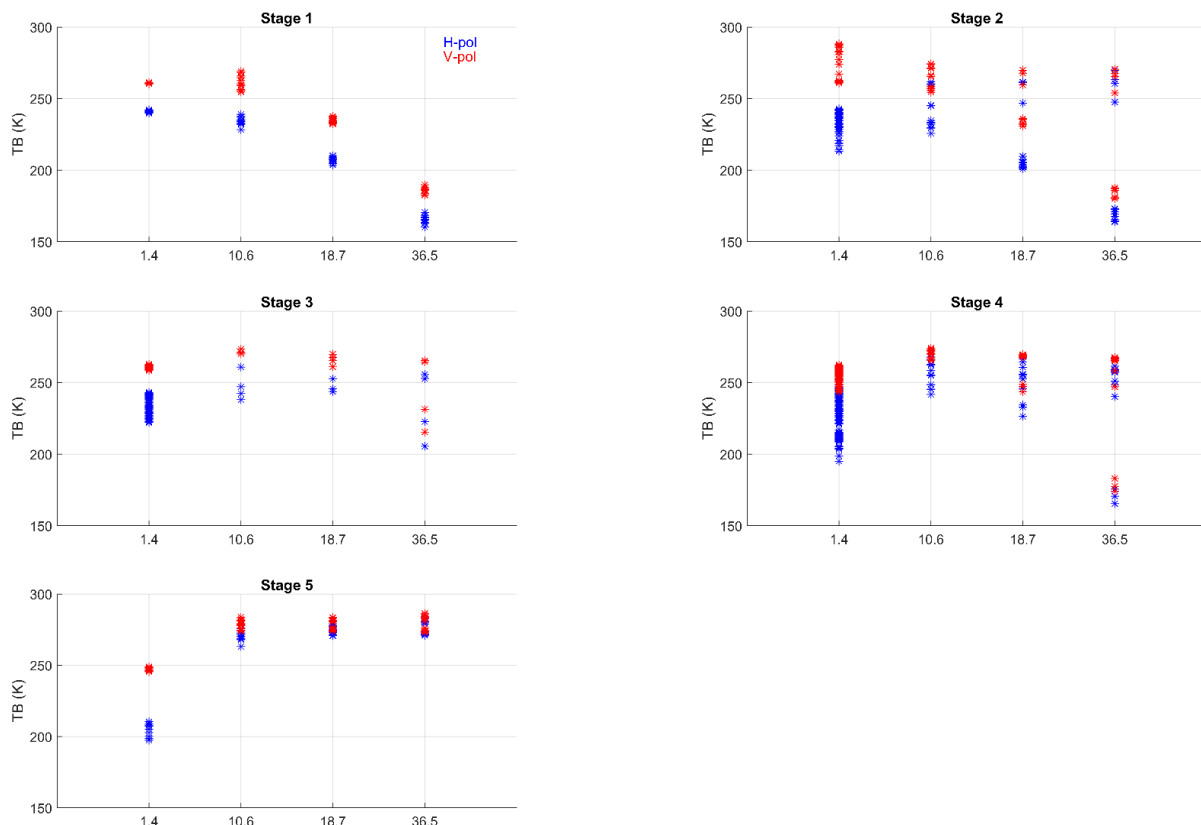


Figure 7: Microwave measurements at four frequencies during different stages of snowmelt and soil thaw: 1: frozen soil, dry snow, 2: wet surface snow, 3: frozen soil, wet snowpack, 4: moist (thawing) soil, wet snowpack, 5) warm (thawed) soil, no snow.

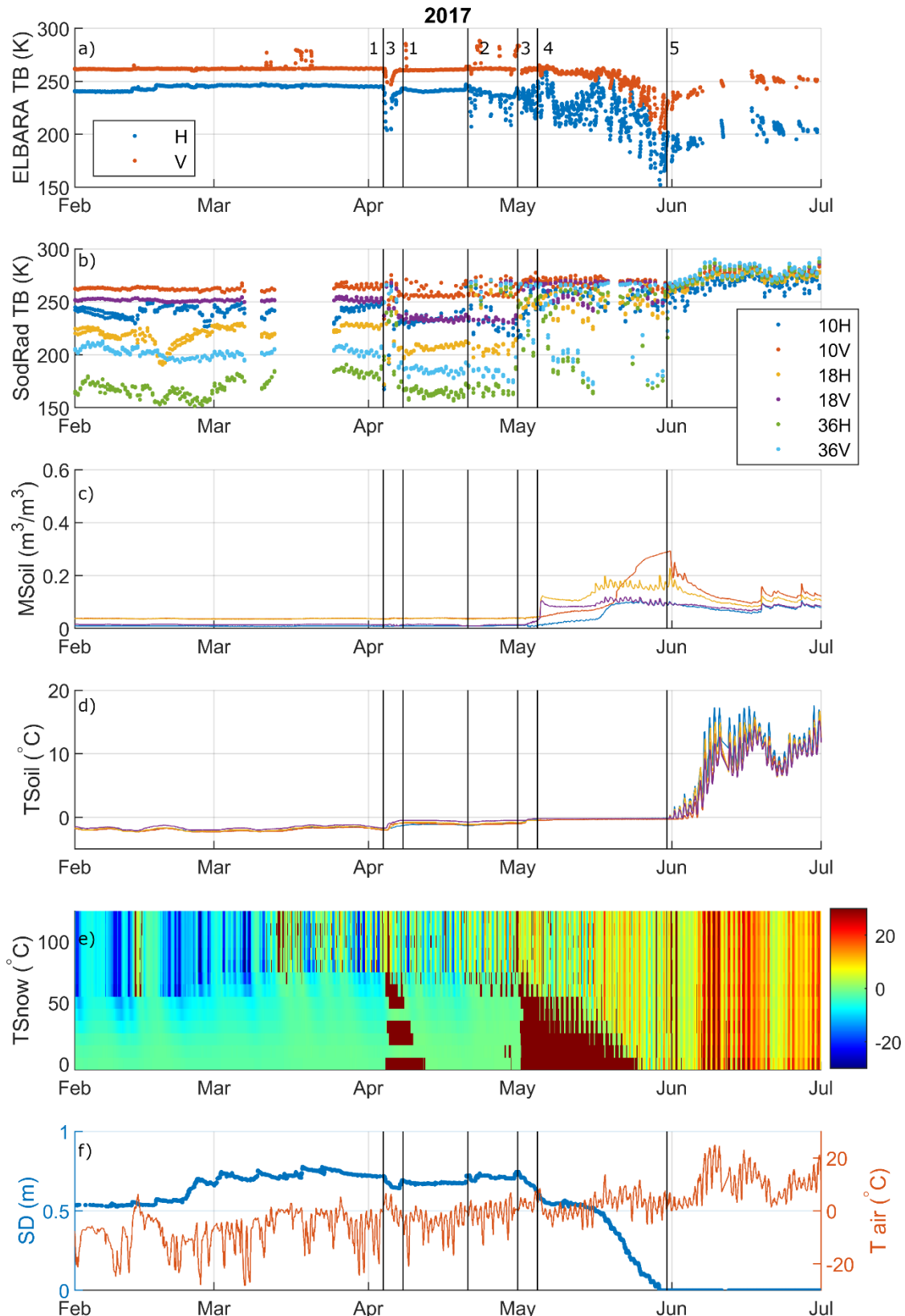


Figure 8: Measurement data of spring 2017: a) ELBARA-II, b) SodRad-1, c) soil surface moisture, d) soil surface temperature, e) snow temperature with wet snow marked with dark red, f) snow depth and air temperature. The stages of soil thaw are marked with numbers 1-5 in a): 1: frozen soil, dry snow, 2: wet surface snow, 3: frozen soil, wet snowpack, 4: moist (thawing) soil, wet snowpack, 5) warm (thawed) soil, no snow.

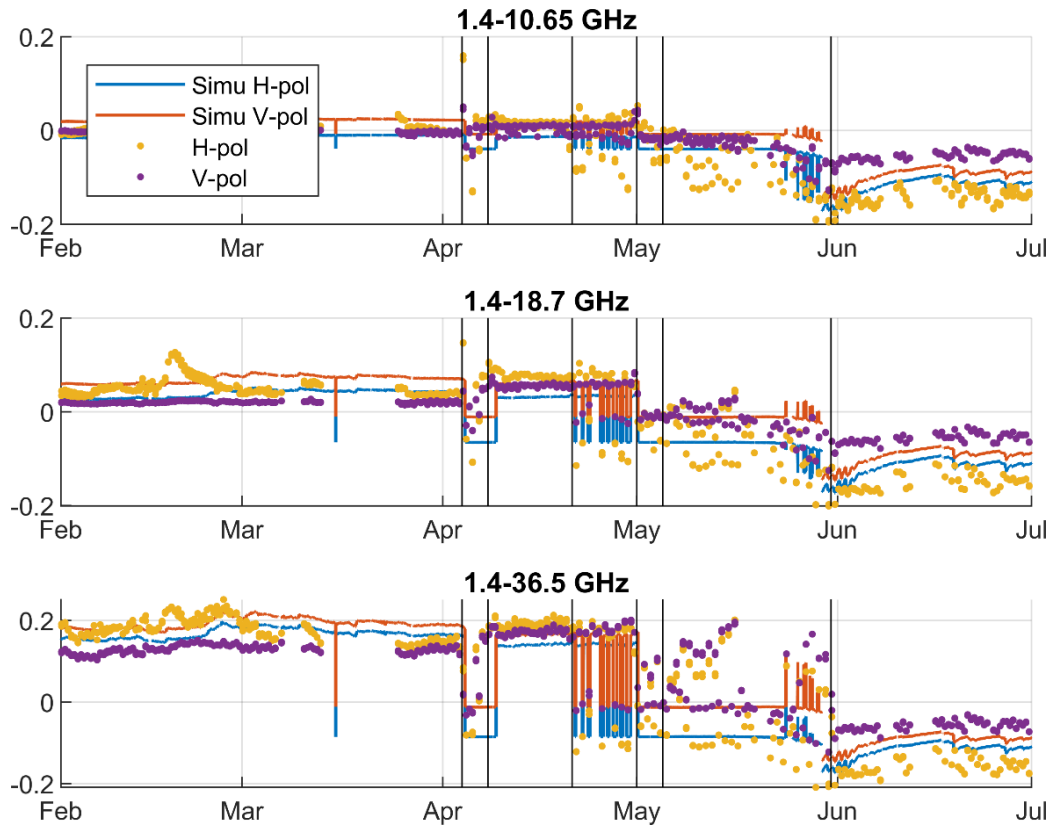


Figure 9: Normalized frequency ratio for two polarizations, simulated (continuous line) and measured (dots).

## 6 DISCUSSION

Multiangl retrievals of forest weren't considered in this study due to inhomogeneity of the forest in the close proximity of the radiometer. The developed L-VOD model was tested for two years, but the change of measurement direction (resulting in change of biomass in the field of view) made it difficult to estimate how well the model fitted with measurements of one year could be applied in longer term. Clearly some of the model parameters, such as amount of water in tree could depend on the water available for the vegetation. Also in long term the trees grow and column mass of wood material could change. Long-term applicability of the model still needs to be tested.

Different existing methods for the retrieval of soil freeze/thaw status from L-band and multifrequency microwave observations was tested, and some new possible methods were identified. One thing that was not considered is the spatial resolution of satellite data. While soil freezing usually is fairly homogeneous, snowmelt and soil thawing have much higher spatial variability due to e.g. warming effect of trees and other objects protruding from snow absorbing solar radiation. While in the small scale of tower-based measurements it is possible to identify exactly the timing of soil thawing, it is not instantaneous in the satellite resolution. This needs to be tested and considered in the future work.

## 7 REFERENCES

- Derksen, C., Xu, X., Scott Dunbar, R., Colliander, A., Kim, Y., Kimball, J. S., Black, T. A., Euskirchen, E., Langlois, A., Lorant, M. M., Marsh, P., Rautiainen, K., Roy, A., Royer, A., & Stephens, J. (2017). Retrieving landscape freeze/thaw state from Soil Moisture Active Passive (SMAP) radar and radiometer measurements. *Remote Sensing of Environment*, *194*, 48–62. <https://doi.org/10.1016/j.rse.2017.03.007>
- Kim, Y., Kimball, J. S., Glassy, J., & Du, J. (2017). An extended global Earth system data record on daily landscape freeze-thaw status determined from satellite passive microwave remote sensing. *Earth System Science Data*, *9*(1), 133–147. <https://doi.org/10.5194/essd-9-133-2017>

# Living Planet Fellowship

- Kim, Y., Kimball, J. S., Xu, X., Dunbar, R. S., Colliander, A., & Derksen, C. (2019). Global assessment of the SMAP freeze/thaw data record and regional applications for detecting spring onset and frost events. *Remote Sensing*, 11(11), 1–24. <https://doi.org/10.3390/rs11111317>
- Klein, L., & Swift, C. (1977). An improved model for the dielectric constant of sea water at microwave frequencies. *IEEE Transactions on Antennas and Propagation*, 2(1), 104–111. <https://doi.org/10.1109/JOE.1977.1145319>
- Li, Q., Kelly, R., Leppanen, L., Vehvilainen, J., Kontu, A., Lemmetyinen, J., & Pulliainen, J. (2019). The Influence of Thermal Properties and Canopy-Intercepted Snow on Passive Microwave Transmissivity of a Scots Pine. *IEEE Transactions on Geoscience and Remote Sensing*, 57(8). <https://doi.org/10.1109/TGRS.2019.2899345>
- Lintunen, A., Hölttä, T., & Kulmala, M. (2013). Anatomical regulation of ice nucleation and cavitation helps trees to survive freezing and drought stress. *Scientific Reports*, 3, 1–7. <https://doi.org/10.1038/srep02031>
- Mätzler, C. (1987). Applications of the interaction of microwaves with the natural snow cover. *Remote Sensing Reviews*, 2(2), 259–387. <https://doi.org/10.1080/02757258709532086>
- Mätzler, C. (1994). Microwave transmissivity of a forest canopy - Experiments made with a beech. *Remote Sensing of Environment*, 48(2), 172–180.
- Mätzler, C. (2006). *Thermal Microwave Radiation: Applications for Remote Sensing*. IEE Electromagnetic Waves series No. 52.
- Muzalevskiy, K., Ruzicka, Z., Roy, A., Loranty, M., & Vasiliev, A. (2022). *Brief communication : Classification of thawed / frozen topsoil state by spectral gradient methods based on SMAP and GCOM-W1 radiometric data*. 30(July), 1–11.
- Rautiainen, K., Parkkinen, T., Lemmetyinen, J., Schwank, M., Wiesmann, A., Ikonen, J., Derksen, C., Davydov, S., Davydova, A., Boike, J., Langer, M., Drusch, M., & Pulliainen, J. (2016). SMOS prototype algorithm for detecting autumn soil freezing. *Remote Sensing of Environment*, 180, 346–360. <https://doi.org/10.1016/j.rse.2016.01.012>
- Roy, A., Toose, P., Mavrovic, A., Pappas, C., Royer, A., Derksen, C., Berg, A., Rowlandson, T., El-Amine, M., Barr, A., Black, A., Langlois, A., & Sonnentag, O. (2020). L-Band response to freeze/thaw in a boreal forest stand from ground- and tower-based radiometer observations. *Remote Sensing of Environment*, 237(November 2019), 111542. <https://doi.org/10.1016/j.rse.2019.111542>
- Schwank, M., Kontu, A., Mialon, A., Naderpour, R., Houtz, D., Lemmetyinen, J., Rautiainen, K., Li, Q., Richaume, P., Kerr, Y., & Mätzler, C. (2021). Temperature effects on L-band vegetation optical depth of a boreal forest. *Remote Sensing of Environment*, 263, 112542. <https://doi.org/10.1016/j.rse.2021.112542>
- Schwank, M., Naderpour, R., & Mätzler, C. (2018). “Tau-Omega” - and two-stream emission models used for passive L-band retrievals: Application to close-range measurements over a forest. *Remote Sensing*, 10(1868). <https://doi.org/10.3390/rs10121868>
- Schwank, M., Wiesmann, A., Werner, C., Mätzler, C., Weber, D., Murk, A., Völksch, I., & Wegmüller, U. (2010). ELBARA II, an L-band radiometer system for soil moisture research. *Sensors*, 10(1), 584–612. <https://doi.org/10.3390/s100100584>
- Wang, P., Zhao, T., Shi, J., Hu, T., Roy, A., Qiu, Y., & Lu, H. (2019). Parameterization of the freeze/thaw discriminant function algorithm using dense in-situ observation network data. *International Journal of Digital Earth*, 12(8), 980–994. <https://doi.org/10.1080/17538947.2018.1452300>
- Wiesmann, A., & Mätzler, C. (1999). Microwave emission model of layered snowpacks. *Remote Sensing of Environment*, 70(3), 307–316. [https://doi.org/10.1016/S0034-4257\(99\)00046-2](https://doi.org/10.1016/S0034-4257(99)00046-2)
- Zhao, T., Shi, J., Zhao, S., Wang, P., Li, S., Ziong, C., & Ziao, Q. (2017). Multi-frequency microwave radiometric measurements of soil freeze-thaw process over seasonally frozen ground. *2017 IEEE International Geoscience and Remote Sensing Symposium (IGARSS)*.